NANO LETTERS

pubs.acs.org/NanoLett Letter

# Disentangling the Effects of Laser and Electron Irradiation on AgX (X = Cl, Br, and I): Insights from Quantum Chemical Calculations

Luis Cabral,* Edson R. Leite, Elson Longo, Miguel A. San-Miguel, Edison Z. da Silva, and Juan Andrés*

Cite This: https://doi.org/10.1021/acs.nanolett.3c04130 Read Online

ACCESS | Metrics & More | Article Recommendations | Supporting Information

**ABSTRACT:** The effects on the lattice structure and electronic properties of different polymorphs of silver halide, AgX (X = Cl, Br, and I), induced by laser irradiation (LI) and electron irradiation (EI) are investigated using a first-principles approach, based on the electronic temperature ($T_e$) within a two-temperature model (TTM) and by increasing the total number of electrons ($N_e$), respectively. *Ab initio* molecular dynamics (AIMD) simulations provide a clear visualization of how $T_e$ and $N_e$ induce a structural and electronic transformation process during LI/EI. Our results reveal the diffusion processes of Ag and X ions, the amorphization of the AgX lattices, and a straightforward interpretation of the time evolution for the formation of Ag and X nanoclusters under high values of $T_e$ and $N_e$. Overall, the present work provides fine details of the underlying mechanism of LI/EI and promises to be a powerful toolbox for further cross-scale modeling of other semiconductors.

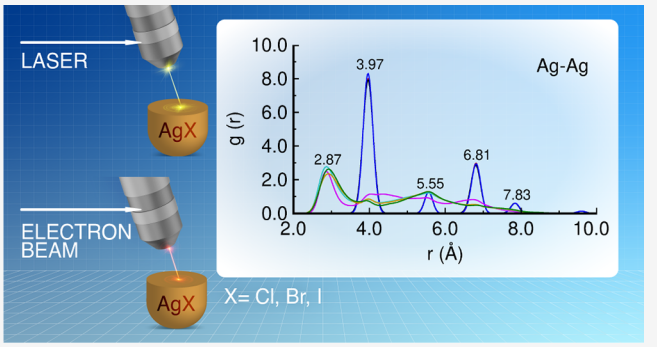


**KEYWORDS:** *Silver halides, AgX (X = Cl, Br, and I), laser and electron irradiation, two-temperature model, ab initio molecular dynamics simulations*



Light/particle interactions in the forms of electromagnetic waves and particle beams, especially in atomically precise nanomaterials, belong to an unexplored realm of research.[1−3] In recent years, laser irradiation (LI) and electron irradiation (EI) of materials have become powerful and innovative tools for modification of materials at the nano/atomic scales, which inspire fundamental research focused on potential technological applications.[4−12] Both LI and EI offer unique capabilities to energize semiconducting inorganic materials with high efficiency and environmental friendliness (high purity, absence of byproducts, simplicity, nontoxicity, and the elimination of the need for surfactants and reducing agents) out of the thermodynamic equilibrium.

Specifically, LI applied to the material supplies the energy needed to induce electronic excitations that can significantly modify the material properties. On the other hand, EI can be precisely focused on the nanoscale using optical components, with energy transferred to the target area through the inelastic scattering of incident electrons.[13] In these processes, electrons become rapidly excited (within a few tens of femtoseconds), contrasting with the heat diffusion time scale. Subsequently, the high electronic energy dissipates into the lattice. It leads to the heating of the lattice until the electrons and lattice reach thermodynamic equilibrium via an electron−phonon coupling process.[14,15]

LI and EI processes are governed by a complex interplay between thermodynamics and kinetics, wherein the excess of energy distorts the lattice structure, inducing growth and crystallization of the materials.[16,17] Characterization of the nature and spatial extent of structural disorder and electronic changes induced by LI and EI evades most of the experimentally available techniques.[18] Quantum mechanical simulations, based on first-principles calculations, have full access to these phenomena at atomistic scale[19] but face the challenge of accurately sampling high-dimensional configuration spaces to identify the thermodynamic and kinetic conditions that impact material properties. Our group is engaged in a research project involving experiments and first-principles calculations and simulations to achieve a comprehensive understanding and develop predictive models for the far-from-equilibrium effects on structure and properties provoked by LI/EI on semiconductors to guide the synthesis of the irradiated materials with desirable applications.

A pioneering effort involved the direct observation of the formation of Ag nanoparticles (NPs) on the surface of various silver-based materials under EI, such as $Ag_2WO_4$,[20,21] *β*-

Received: October 27, 2023
Revised: January 17, 2024
Accepted: January 18, 2024




https://doi.org/10.1021/acs.nanolett.3c04130
Nano Lett. XXXX, XXX, XXX−XXX

$Ag_2WO_4$,[22,23] $\beta$-$Ag_2MoO_4$,[24,25] $Ag_3PO_4$,[26] $\beta$-$AgVO_3$,[27] $Ag_2CrO_4$,[28] and AgX (X = Cl, Br, and I)[29] crystals and additionally, In NPs and Bi NPs in InP[30,31] and $NaBiO_3$,[32,33] respectively. The ability to conduct in situ atomic-scale observations combined with simulations based on first-principles calculations in nanomaterials enables the atomic-scale recording of events,[34] providing new insights into the mechanism of the Ag NP growth process. This novel phenomenon opens a new window for synthesizing and exploring promising composite materials in materials science and nanotechnology, offering an innovative, straightforward, and highly efficient synthesis of NPs and nanocomposites. In this context, a scalable electron beam irradiation platform has been developed by EI to obtain innovative materials for technological and industrial applications.[35]

Considering the aforementioned factors, it is evident that enhancing our comprehension of the response exhibited by materials subjected to LI and EI is a prominent research area spanning fundamental exploration to practical technological applications. In the present work, we study the change in the structural and electronic properties and the mechanisms involved in the LI and EI on AgX (X = Cl, Br, and I) polymorphs. The two-temperature model (TTM) is selected[36] to simulate the effect of LI, which adopts finite-temperature density functional theory (FT-DFT)[37−39] and the electronic temperature ($T_e$)[40] to describe the electron excitation. This computational strategy has been successfully employed to investigate the effects of LI on metals and semiconductors.[41,42] The modifications induced by EI are investigated by adding electrons ($N_e$) in the AgX polymorphs. Thereafter, *ab initio* molecular dynamics (AIMD) simulations have been performed to analyze the time evolution of these properties under electronic excitations and the addition of electrons, see the Methods section in the Supporting Information (SI). We have selected AgCl and AgBr with rock salt and zinc blend structures, while for AgI, the wurtzite polymorph has also been considered.

There is a second goal in this work. We want to clarify the differences and similarities in the changes induced by the nonequilibrium processes of both types of irradiation. These results extend the fundamental understanding of the underlying mechanisms of LI and EI on AgX crystals by increasing $T_e$ and $N_e$ in the bulk structure. Thus, our findings provide viable guidance for realizing new materials for multifunctional applications. We, therefore, present a workflow based on DFT simulations with the modest but crucial goal of clarifying the differences and similarities in the changes induced by both types of irradiation along the nonequilibrium processes.

The two key advances addressed in this paper are as follows. First, we evaluate the changes in structure and electronic properties and extend the fundamental understanding of the underlying mechanism induced by LI and EI on AgX crystals. Second, this work reveals the potential of the present methods and computational techniques to provide some fundamental insights to deepen understanding of the effects of LI and EI on the structure and electronic properties of a broad spectrum of materials, which provides further viable guidance for developing new materials for frontier applications.

The optimized, experimental, and previous results of other DFT calculations for the lattice parameters of the equilibrium structures of AgX (X = Cl, Br, and I) polymorphs are presented in Table S1 for comparison purposes. Also, the band gap values are shown in Table S2. In addition to the observed overestimation of lattice parameters and underestimation of band gap values by the GGA-PBE exchange and correlation energy functional,[43,44] this study primarily centers on investigating the impacts of $T_e$ and $N_e$. It is important to note that the discussion regarding the trends in structural and electronic properties induced by LI and EI is expected to remain largely unaffected by this overestimation/underestimation. However, it should be recognized that the specific values of $T_e$ and $N_e$ that trigger changes in the structure and electronic properties might be influenced by these discrepancies. The GGA-PBE calculations indicate that the stability order for AgCl and AgBr systems are as follows: rock-salt > zinc-blend, while in AgI, it is wurtzite ≥ zinc-blend > rock-salt, as shown in Table S2.

A material under LI/EI may experience a heat transfer process to increase the temperature ($T$), with significant changes in the lattice structure and electronic properties. To describe this effect, the variation of $T$ at different values of $T_e$ and $N_e$ in the range from 0 to 5.0 ps for AgX is presented in Figures S1−S6. An analysis of the results points out two thresholds constituting the lower limit for the $T_e$ (LI) and $N_e$ (EI) values. Below these values, the electronic excitations and electron additions are insufficient to increase $T$ along the AIMD simulations. These thresholds are 2.00 eV and 8e (AgCl, rock-salt); 1.00 eV and 2e (AgCl, zinc-blend); 2.00 eV and 9e (AgBr, rock-salt); 1.00 eV and 2e (AgBr, zinc-blend); 2.00 eV and 12e (AgI, rock-salt); 2.00 eV and 7e (AgI, zinc-blend); 2.00 eV, and 6e (AgI, wurtzite). Due to symmetry, a smaller external energy is enough to provoke the lattice changes in the AgCl and AgBr in the zinc-blend phase, while AgI in the zinc-blend and wurtzite phases shows similar values of LI.

The average $T$ values below specific thresholds are reported in Table S3. Above these limits, there is a sudden change in the $T$ values as $T_e$ and $N_e$ increase, and the "hot" electrons heat the AgX lattice; their structural changes are sufficiently stabilized along the AIMD simulation. When the temperature reaches a specific temperature range, the crystal is perturbed, and we find that the most stable zinc-blend polymorphs of both AgCl and AgBr need smaller values of $T_e$ and $N_e$ to heat the lattice with respect to the rock-salt polymorph. A similar behavior was found for wurtzite and zinc-blend compared to rock-salt AgI polymorphs. We can sense that LI reaches a higher $T$ value than EI, as presented in Table S4. Accepting electrons until $N_e$ = 12e, 7e, and 6e in the AgI rock-salt, AgI zinc-blend, and AgI wurtzite under EI, respectively, maintains $T$ within a particular time along the AIMD simulation. For these systems, we found that the $N_e$ threshold becomes lower with decreasing the AIMD simulation. Interestingly, the $N_e$ threshold decreases with the simulation time for these systems, indicating that the lattice remains unchanged as electrons are injected for approximately 1.5, 1.0, and 0.5 ps, respectively. These changes result from excess energy activating the bending and stretching modes of the AgX lattice. The results suggest that the AgBr rock-salt lattice under EI is more robust, exhibiting greater resistance to electron injection compared to the AgBr zinc-blend. However, this behavior differs for AgI; the zinc-blend can accommodate more electrons than the wurtzite and rock-salt polymorphs before their corresponding lattices are heated.

Therefore, we can divide the excitation process into two steps. First, the energy induced by LI/EI is coupled to electrons within a very short period, on the order of sub-picosecond, during which the lattice remains undisturbed and cool. In the second stage, as the temperature increases sufficiently, changes in material structure and properties occur due to exposure to LI/EI. These changes arise from electron−electron scattering and


https://doi.org/10.1021/acs.nanolett.3c04130
Nano Lett. XXXX, XXX, XXX−XXX

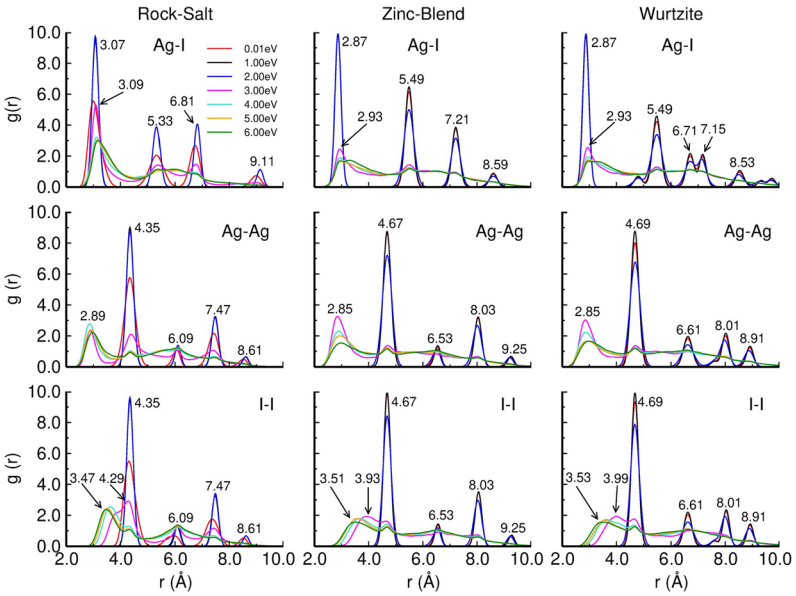


**Figure 1.** Pair correlation functions obtained from AIMD simulations under LI at 5.0 ps for Ag−I, Ag−Ag, and I−I distances at different $T_e$ in rock-salt, zinc-blend, and wurtzite phases.

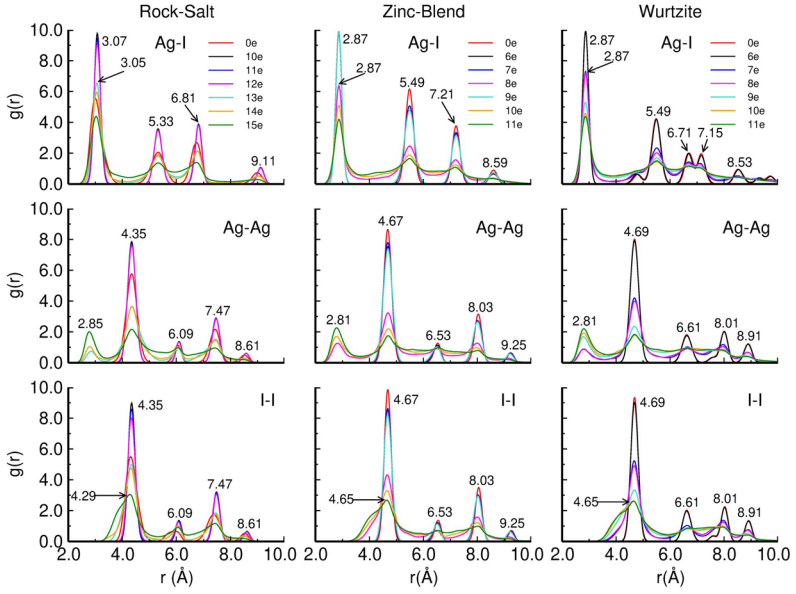


**Figure 2.** Pair correlation functions obtained from AIMD simulations under EI at 5.0 ps for Ag−I, Ag−Ag, and I−I distances at different $N_e$ in rock-salt, zinc-blend, and wurtzite phases.

electron−phonon coupling, providing energy to the lattice and resulting in crystal heating. Previous results suggest that lattice modification occurs when $T_e$ and $N_e$ surpass a threshold during LI/EI.[31,41,45,46] To understand the mechanism of the heat modification, we calculated the pair correlation function $g(r)$, the mean square displacement (MSD), and the diffusion coefficient ($D$).

An analysis of the $g(r)$ profiles applies to crystalline and amorphous materials to obtain deep insight into the integrity of the lattice structure during the LI/EI of the different polymorphs.[47,48] The results for AgCl and AgBr are presented in Figures S7−S10, while the $g(r)$ for the three polymorphs of AgI are displayed in Figure 1 for LI and Figure 2 for EI. The prominent $g(r)$ peaks correspond to the average first, second, third, and fourth coordination shells of Ag−X, Ag−Ag, and X−X distances. These profiles reveal that the Ag and X ions maintain the ordered lattice structure until specific values of $T_e$ and $N_e$ are reached, i.e., 3.00 eV and 9e (AgCl, rock-salt); 2.00 eV and 3e (AgCl, zinc-blend); 3.00 eV and 10e (AgBr, rock-salt); 2.00 eV and 3e (AgBr, zinc-blend); 3.00 eV and 13e (AgI, rock-salt); 3.00 eV and 8e (AgI, zinc-blend); 3.00 eV and 7e (AgI, wurtzite).

Under these thresholds, the lattice remains robust, and the Ag−X, Ag−Ag, and X−X distances fluctuate near the equilibrium bond length for all. The lattice cannot be perturbed, because the excess of energy is insufficient to modify their structure, and there are no substantial differences in the $g(r)$ profiles. For higher values of $T_e$ and $N_e$, an abrupt change occurs, in which the maximum peak for the first coordination shell, corresponding to the Ag−X, Ag−Ag, and X−X distances,


https://doi.org/10.1021/acs.nanolett.3c04130
Nano Lett. XXXX, XXX, XXX−XXX

**Table 1. Calculated Values of the Ag−X, Ag−Ag, and X−X Distances Corresponding to Peaks of Pair Correlation Function for Unperturbed Lattices, in Rock-Salt (AgCl, AgBr, AgI), Zinc-Blend (AgCl, AgBr, AgI), and Wurtzite (AgI) Lattices**

| | rock-salt | | | zinc-blend | | | wurtzite |
|---|---|---|---|---|---|---|---|
| | AgCl | AgBr | AgI | AgCl | AgBr | AgI | AgI |
| Ag−X | 2.81, 4.85, 6.21, 8.33 | 2.91, 5.05, 6.47, 8.67 | 3.07, 5.33, 6.81, 9.11 | 2.63, 5.01, 6.59, 7.87 | 2.73, 5.23, 6.87, 8.19 | 2.87, 5.49, 7.21, 8.59 | 2.87, 5.49, 6.71, 7.15, 8.53 |
| Ag−Ag | 3.97, 5.55, 6.81, 7.83 | 4.13, 5.79, 7.09, 8,17 | 4.35, 6.09, 7.47, 8.61 | 4.29, 5.97, 7.33, 8.42 | 4.47, 6.21, 7.65, 8.79 | 4.67, 6,53, 8.03, 9,25 | 4.69, 6.61, 8.01, 8.91 |
| X−X | 3.97, 5.55, 6.81, 7.83 | 4.13, 5.79, 7.09, 8,17 | 4.35, 6.09, 7.47, 8.61 | 4.29, 5.97, 7.33, 8.42 | 4.47, 6.21, 7.65, 8.79 | 4.67, 6,53, 8.03, 9,25 | 4.69, 6.61, 8.01, 8.91 |

**Table 2. Calculated Values of the Ag−X, Ag−Ag, and X−X Distances Corresponding to Peaks of Pair Correlation Function for Perturbed Lattices, in Rock-Salt (AgCl, AgBr), Zinc-Blend (AgCl, AgBr), and Wurtzite (AgCl, AgBr, AgI) Lattices under LI and EI**

| | rock-salt | | | zinc-blend | | | wurtzite |
|---|---|---|---|---|---|---|---|
| | AgCl | AgBr | AgI | AgCl | AgBr | AgI | AgI |
| Ag−X | | | | | | | |
| LI: | 2.79 | 2.91 | 3.09 | 2.61 | 2.75 | 2.93 | 2.93 |
| EI: | 2.73 | 2.91 | 3.05 | 2.63 | 2.73 | 2.87 | 2.87 |
| Ag−Ag | | | | | | | |
| LI: | 2.87 | 2.87 | 2.89 | 2.87 | 2.87 | 2.85 | 2.85 |
| EI: | 2.81 | 2.85 | 2.85 | 2.91 | 2.81 | 2.81 | 2.81 |
| X−X | | | | | | | |
| LI: | 2.97−3.47 | 3.17−3.59 | 3.47−4.29 | 3.03−4.21 | 3.25−3.69 | 3.51−3.93 | 3.53−3.99 |
| EI: | 3.43−3.59 | 3.67−4.11 | 4.29−4.33 | 4.17−4.25 | 4.39−4.43 | 4.65−4.67 | 4.65−4.67 |

**Table 3. Calculated Values of $g(r)$ Peaks for Unperturbed Lattices Corresponding to the First, Second, Third, And Fourth Coordination Shells of Ag−X, Ag−Ag, and X−X, in Rock-Salt (AgCl, AgBr, AgI), Zinc-Blend (AgCl, AgBr, AgI) and Wurtzite (AgI) Lattices**

| | rock-salt | | | zinc-blend | | | wurtzite |
|---|---|---|---|---|---|---|---|
| | AgCl | AgBr | AgI | AgCl | AgBr | AgI | AgI |
| Ag−X | 9.26, 3.54, 3.75, 1.00 | 9.50, 3.71, 3.89, 1.03 | 9.74, 3.81, 4.01, 1.06 | 8.98, 5.05, 3.04, 0.67 | 9.33, 5.28, 3.35, 0.78 | 9.99, 6.51, 3.84, 0.92 | 9.99, 4.57, 2.17, 2.09, 1.07 |
| Ag−Ag | 8.30, 1.26, 2.85, 0.60 | 8.58, 1.32, 2.97, 0.56 | 9.02, 1.14, 3.25, 0.66 | 7.28, 1.08, 2.63, 0.55 | 7.66, 1.34, 2.79, 0.61 | 8.64, 1.36, 3.22, 0.64 | 8.76, 1.96, 2.18, 1.34 |
| X−X | 8.57, 1.24, 2.86, 0.57 | 8.92, 1.30, 3.12, 0.63 | 9.63, 1.28, 3.38, 0.67 | 8.33, 1.19, 2.92, 0.60 | 8.62, 1.23, 3.09, 0.63 | 9.85, 1.40, 3.46, 0.63 | 9.91, 2.20, 2.24, 1.44 |

decreases, while the second and third peaks of $g(r)$ disappear. It should be noted that the first peak shifts toward lower values of Ag−X, Ag−Ag, and X−X distances, while its intensity decreases as $T_e/N_e$ increases. This behavior indicates that the Ag and X species maintain their preferred local coordination, while the broadening of the peaks reflects an increased local structural disorder. Despite this disorder, the crystals exhibit a degree of chemical short-range order.

Beyond this threshold, the $g(r)$ profile of the first peak becomes flatter when $T_e$ and $N_e$ increase, resulting in the loss of medium- and long-range order of the Ag and X ion sublattice, while the first coordination shell of the Ag and X ions is maintained. This short-range order can be related to local changes in the nearest-neighbor bond lengths associated with distinct coordination environments. The excitation and additional electrons break the ground-state balance between atoms and electrons, thus producing mechanical stresses and forces leading to a significant degree of structural disorder. This structural evolution can be associated with an order−disorder transition involving the amorphization of the lattice. Tables 1 and 2 present the values of the $g(r)$ peaks related to Ag−X, Ag−Ag, and X−X distances in the different unperturbed and perturbed polymorphs of AgX, respectively.

For AgCl in both rock-salt and zinc-blend polymorphs, the first $g(r)$ peak of the Ag−Ag distance shifts from 3.97 and 4.29 Å in the unperturbed lattice to 2.87 and 2.81 Å and 2.87 and 2.91 Å in the perturbed lattice under LI and EI, respectively. Similar changes are observed for AgBr and AgI polymorphs, indicating a higher displacement of Ag cations in zinc-blend compared to rock-salt polymorphs to form the mentioned structural motifs. Dixon reported the structures of small $Ag_n$ clusters, $(Ag)_n$, $n <$ 100, showing that the average Ag−Ag bond length of $Ag_7$ to $Ag_{14}$ ranges from 2.85 to 2.89 Å.[49] In addition, these values are close to the value of 2.89 Å for the bulk Ag structure with $Fm3m$ symmetry.[50] These results suggest the presence of small clusters or nanodomains of $Ag_n$ ($n$ = 7−14) and/or solid Ag. Our research group has previously observed similar behavior, where EI on $\alpha$-$Ag_2WO_4$ generates the formation of metallic Ag NPs.[51−53] It is important to note that despite the different nature of irradiation in both LI and EI and the structural differences in the AgX polymorphs, the Ag−Ag values indicate the presence of tiny clusters of $Ag_n$ ($n$ = 7−14) and/or solid Ag. The first $g(r)$ peak corresponding to the Br−Br distance of AgBr structure in rock-salt and zinc-blend phases under EI and LI is shifted from 4.13 and 4.47 Å to shorter distances of 2.87 and 2.85 Å and 2.87 and 2.81 Å, respectively. For AgI under LI and EI, the first $g(r)$


https://doi.org/10.1021/acs.nanolett.3c04130
Nano Lett. XXXX, XXX, XXX−XXX

Table 4. Calculated Values of $g(r)$ Peaks for the Ag−X, Ag−Ag, and X−X under LI and EI, in Rock-Salt (AgCl, AgBr, AgI), Zinc-Blend (AgCl, AgBr, AgI), and Wurtzite (AgI) Lattices

| | rock-salt | | | zinc-blend | | | wurtzite |
|---|---|---|---|---|---|---|---|
| | AgCl | AgBr | AgI | AgCl | AgBr | AgI | AgI |
| Ag−X | | | | | | | |
| LI: | 3.53 | 3.81 | 5.47 | 5.41 | 6.57 | 2.42 | 2.42 |
| EI: | 3.48 | 7.26 | 6.55 | 5.92 | 7.67 | 6.39 | 7.30 |
| Ag−Ag | | | | | | | |
| LI: | 2.77 | 3.07 | 2.76 | 2.96 | 2.88 | 3.26 | 3.03 |
| EI: | 2.31 | 2.29 | 1.86 | 1.98 | 2.01 | 2.25 | 2.21 |
| X−X | | | | | | | |
| LI: | 2.48−2.70 | 2.42−2.48 | 2.38−2.93 | 1.70−2.04 | 1.58−1.82 | 1.53−1.92 | 1.55−1.93 |
| EI: | 2.16−2.21 | 3.67−3.25 | 3.05−5.00 | 2.13−3.86 | 2.19−5.29 | 4.32−2.68 | 2.61−5.23 |

peak in the rock-salt, zinc-blend, and wurtzite for I−I distance is shifted from 4.35, 4.67, and 4.69 Å to shorter distances of 2.89 and 2.85 Å, 2.85 and 2.81 Å, and 2.85 and 2.81 Å, respectively. Hence, it can be concluded that the excitation of electrons induces a more significant structural disorder in comparison to adding electrons.

It is noteworthy that Wu et al.[54,55] and Shi et al.[56] reported an isostructural diatomic molecular phase I (space group of *Cmca*) of the three halogen solids ($Cl_2$, $Br_2$, and $I_2$) in which the values of intermolecular Cl−Cl, Br−Br, and I−I distances are in the ranges of 2.8−3.7 Å. 3.2−3.6 Å, and 3.6−4.25 Å, respectively. Based on these results and the similar values of intermolecular Cl−Cl, Br−Br, and I−I distances, it is possible to suggest the appearance of the nanoclusters of Cl, Br, and I, associated with early stages of the formation of the *Cmca* polymorphs with a lamellar structure where each layer is composed of zigzag chains of diatomic molecules. The values of $g(r)$ peaks for the unperturbed and perturbed AgX lattice under LI and EI are reported in Tables 3 and 4, respectively.

The calculated MSD and $D$ along AIMD simulations in the range of 0−5.0 ps are displayed in Figures S11−S16, and the results are presented and discussed in the SI. In summary, the $g(r)$ peaks, the MSD, and the $D$ values as a function of simulation time point out an abrupt change in the structure of AgX polymorphs at specific $T_e$ and $N_e$ values, revealing a structural order−disorder transition in which only the short-range order is maintained. This change is associated with the crystalline to amorphous transformation of AgX structure with the simultaneous formation of Ag and X nanoclusters. In the SI, there are videos showcasing the evolution of AgX polymorphs under LI and EI at the threshold values. These videos depict the initial crystalline structures and the displacement of Ag and X atoms when the system is heated sufficiently to undergo the transformation to an amorphous structure, followed by the formation of Ag and X clusters.

The relative potential energies at the threshold values along the AIMD simulations are presented in Figures S17 and S18 in the SI for LI and EI, respectively. In the case of LI, all plots exhibit an initial abrupt increase in potential energy attributed to the heating process induced by the excited electrons. This increase persists until reaching an approximate maximum value, signifying the amorphization of the system, as depicted in the plot. The specific time marking the transition from crystalline to amorphous is also highlighted in the supplementary videos. Subsequent fluctuations in potential energy arise as a consequence of diffusion processes and cluster formation. For EI, the potential energy plots initially show an increase, followed by a decrease to a minimum value corresponding to the disordered system. The fluctuating behavior is also a result of diffusion processes and cluster formation.

This study extensively explores the fundamental aspects for understanding the effects of LI and EI on the lattice structure and electronic properties of various polymorphs of AgX under nonequilibrium states through first-principles calculations. Electronic excitations and addition of electrons to these semiconductors, followed by AIMD simulations, indicate that the effects of LI and EI on AgX polymorphs can be divided into three stages: the diffusion process of Ag and X ions, crystal amorphization with maintained short-range order, and formation of Ag and X nanoclusters associated with the breaking of Ag−X bonds under high values of $T_e$ and $N_e$.

The lower threshold values for achieving the amorphization of the AgX lattice in the LI and EI are $T_e$ = 3.00 eV and $N_e$ = 9e (AgCl, rock-salt); $T_e$ = 2.00 eV and $N_e$ = 3e (AgCl, zinc-blend); $T_e$ = 3.00 eV and $N_e$ = 10e (AgBr, rock-salt); $T_e$ = 2.00 eV and $N_e$ = 3e (AgBr, zinc-blend); $T_e$ = 3.00 eV and $N_e$ = 13e (AgI, rock-salt); $T_e$ = 3.00 eV and $N_e$ = 8e (AgI, zinc-blend); $T_e$ = 3.00 eV and $N_e$ = 7e (AgI, wurtzite), respectively. Beyond these threshold values, metallic behavior of Ag and the presence of X clusters under LI/EI are observed. These findings illustrate the relationship between solid thermal evolution and structural and electronic motifs, providing insights into the underlying mechanisms involved during LI/EI.

The current approach holds the potential to be systematically employed in the exploration of other inorganic semiconductors. However, it is crucial to acknowledge the limitations inherent in the current computational methods. Our choice of an intuitive model, utilizing a box of 64 ions to represent the AgX polymorphs, offers a simplified yet valuable perspective that cannot fully replicate all features of these polymorphs. Nevertheless, this theoretical study establishes a framework for systematically analyzing the effects of LI/EI on these semiconductors and extracting essential structural and electronic features that may be challenging to achieve through experimental methods.

Moreover, it is interesting to note that the anticipated results of this work can serve as input data for machine learning and artificial intelligence, facilitating the correlation of structure, properties, and function to predict material properties, construct materials from scratch, and uncover new mechanisms beyond intuition.[57,58] This not only validates and encourages the use of the present methods and techniques but also provides valuable guidance and optimization for realizing new and more efficient materials for multifunctional applications.

Present outcomes have the potential to benefit diverse scientific communities in the fields of materials science, physics,


https://doi.org/10.1021/acs.nanolett.3c04130
Nano Lett. XXXX, XXX, XXX−XXX

chemistry, and engineering technology, offering comprehensive insights into laser- and electron-beam-assisted procedures for next-generation electronic materials and energy.

## ■ ASSOCIATED CONTENT

### Supporting Information

The Supporting Information is available free of charge at https://pubs.acs.org/doi/10.1021/acs.nanolett.3c04130.

Methods; static features of AgX polymorphs; dynamical properties from AIMD simulations; and electronic analysis of systems unperturbed and under LI and EI (PDF)

Videos showcasing the evolution of AgX polymorphs under LI and EI at the threshold values (ZIP)

## ■ AUTHOR INFORMATION


### Corresponding Authors

**Luis Cabral** − *Institute of Physics Gleb Wataghin (IFGW), Universidade Estadual de Campinas, Campinas 13083-859 SP, Brazil; Department of Physical and Analytical Chemistry, University Jaume I (UJI), Castelló 12071, Spain;* orcid.org/0000-0002-4834-0552; Email: lcabral@ifi.unicamp.br

**Juan Andrés** − *Laboratório Nacional de Nanotecnologia (LNNano), CNPEM, Campinas 13083-970 SP, Brazil; Department of Physical and Analytical Chemistry, University Jaume I (UJI), Castelló 12071, Spain;* orcid.org/0000-0003-0232-3957; Email: andres@qfa.uji.es

### Authors

**Edson R. Leite** − *Laboratório Nacional de Nanotecnologia (LNNano), CNPEM, Campinas 13083-970 SP, Brazil; LIEC-CDMF, Department of Chemistry, Universidade Federal de São Carlos, São Carlos 13565-905 SP, Brazil*

**Elson Longo** − *LIEC-CDMF, Department of Chemistry, Universidade Federal de São Carlos, São Carlos 13565-905 SP, Brazil;* orcid.org/0000-0001-8062-7791

**Miguel A. San-Miguel** − *Department of Physical-Chemistry, Institute of Chemistry, Universidade Estadual de Campinas, Campinas 13083-970 SP, Brazil;* orcid.org/0000-0002-6650-7432

**Edison Z. da Silva** − *Institute of Physics Gleb Wataghin (IFGW), Universidade Estadual de Campinas, Campinas 13083-859 SP, Brazil;* orcid.org/0000-0002-2195-0051

Complete contact information is available at: https://pubs.acs.org/10.1021/acs.nanolett.3c04130


### Author Contributions

L.C.: conceptualization, simulations and original draft; J.A., E.L., and M.A.S.M.: formal analysis, writing−review and editing; E.R.L. and E.Z.D.S.−writing review and editing, software, funding acquisition, and project administration. All authors have read and agreed to the published version of the manuscript.

### Notes

The authors declare no competing financial interest.

## ■ ACKNOWLEDGMENTS

This work was financially supported by the Brazilian agencies: FAPESP (Fundação de Amparo à Pesquisa do Estado de São Paulo), grants 2018/20729-9, 2021/09187-2 (L.C.); 2013/07296-2, 2016/23891-6, 2017/26105-4 (E.Z.S., M.S.M., and E.L.). J.A. thanks Generalitat Valenciana (Conselleria de Innovación, Universidades, Ciencia y Sociedad Digital—project CIAICO/2021/122) and Jaume I University (UJI-B2022-56) for financially supporting this research. The authors acknowledge the computational resources of the CENAPAD-SP and CCJDR-UNICAMP and graphic art developed by Henrique Matheus Campos, from the "Laboratório Aberto de Interatividade para Disseminação do Conhecimento Científico e Tecnológico" (LabI).

## ■ REFERENCES


(1) Gonzalez-Martinez, I. G.; Bachmatiuk, A.; Bezugly, V.; Kunstmann, J.; Gemming, T.; Liu, Z.; Cuniberti, G.; Rümmeli, M. H. Electron-Beam Induced Synthesis of Nanostructures: A Review. *Nanoscale* **2016**, *8*, 11340.

(2) Guo, K.; Baidak, A.; Yu, Z. Recent Advances in Green Synthesis and Modification of Inorganic Nanomaterials by Ionizing and Non-Ionizing Radiation. *J. Mater. Chem. A* **2020**, *8*, 23029.

(3) Tanaka, S. I. Control and Modification of Nanostructured Materials by Electron Beam Irradiation. *Quantum Beam Sci.* **2021**, *5*, 23.

(4) Gräf, S. Formation of Laser-Induced Periodic Surface Structures on Different Materials: Fundamentals, Properties and Applications. *Adv. Opt. Technol.* **2020**, *9*, 11.

(5) Florian, C.; Kirner, S. V.; Krüger, J.; Bonse, J. Surface Functionalization by Laser-Induced Periodic Surface Structures. *J. Laser Appl.* **2020**, *32*, 022063.

(6) Bonse, J.; Gräf, S. Maxwell Meets Marangoni—A Review of Theories on Laser-Induced Periodic Surface Structures. *Laser Photonics Rev.* **2020**, *14*, 1.

(7) Miao, Y.; Tsapatsis, M. Electron Beam Patterning of Metal-Organic Frameworks. *Chem. Mater.* **2021**, *33*, 754.

(8) Jiang, N. Electron Beam Damage in Oxides: A Review. *Rep. Prog. Phys.* **2016**, *79*, 016501.

(9) Xiong, W.; et al. Laser-Based Micro/Nanofabrication in One, Two and Three Dimensions. *Front. Optoelectron.* **2015**, *8*, 351.

(10) Garcia-Lechuga, M.; Puerto, D.; Fuentes-Edfuf, Y.; Solis, J.; Siegel, J. Ultrafast Moving-Spot Microscopy: Birth and Growth of Laser-Induced Periodic Surface Structures. *ACS Photonics* **2016**, *3*, 1961.

(11) Malinauskas, M.; Žukauskas, A.; Hasegawa, S.; Hayasaki, Y.; Mizeikis, V.; Buividas, R.; Juodkazis, S. Ultrafast Laser Processing of Materials: From Science to Industry. *Light Sci. Appl.* **2016**, *5*, e16133.

(12) Zhang, D.; Gökce, B.; Barcikowski, S. Laser Synthesis and Processing of Colloids: Fundamentals and Applications. *Chem. Rev.* **2017**, *117*, 3990.

(13) Jiang, N. Electron Irradiation Effects in Transmission Electron Microscopy: Random Displacements and Collective Migrations. *Micron* **2023**, *171*, 103482.

(14) Kumar, A.; Pollock, T. M. Mapping of Femtosecond Laser-Induced Collateral Damage by Electron Backscatter Diffraction. *J. Appl. Phys.* **2011**, *110*, 083114.

(15) Shugaev, M. V.; Gnilitskyi, I.; Bulgakova, N. M.; Zhigilei, L. V. Mechanism of Single-Pulse Ablative Generation of Laser-Induced Periodic Surface Structures. *Phys. Rev. B* **2017**, *96*, 205429.

(16) Dieperink, M.; Scalerandi, F.; Albrecht, W. Correlating Structure, Morphology and Properties of Metal Nanostructures by Combining Single-Particle Optical Spectroscopy and Electron Microscopy. *Nanoscale* **2022**, *14*, 7460.

(17) Zhang, X.; Zhang, L.; Mironov, S.; Xiao, R.; Guo, L.; Huang, T. Effect of Crystallographic Orientation on Structural Response of Silicon to Femtosecond Laser Irradiation. *Appl. Phys. A Mater. Sci. Process.* **2021**, *127*, 196.

(18) Gilbert, M. R.; et al. Perspectives on Multiscale Modelling and Experiments to Accelerate Materials Development for Fusion. *J. Nucl. Mater.* **2021**, *554*, 153113.

(19) Zhang, Y.; Weber, W. J. Ion Irradiation and Modification: The Role of Coupled Electronic and Nuclear Energy Dissipation and Subsequent Nonequilibrium Processes in Materials. *Appl. Phys. Rev.* **2020**, *7*, 041307.

(20) Assis, M.; et al. Towards the Scale-up of the Formation of Nanoparticles on $\alpha$-Ag2WO4with Bactericidal Properties by Femtosecond Laser Irradiation. *Sci. Rep.* **2018**, *8*, 1884.
(21) Macedo, N. G.; et al. Tailoring the Bactericidal Activity of Ag Nanoparticles/$\alpha$-Ag2WO4 Composite Induced by Electron Beam and Femtosecond Laser Irradiation: Integration of Experiment and Computational Modeling. *ACS Appl. Bio Mater.* **2019**, *2*, 824.
(22) Roca, R. A.; Gouveia, A. F.; Lemos, P. S.; Gracia, L.; Andrés, J.; Longo, E. Formation of Ag Nanoparticles on $\beta$-Ag2WO4 through Electron Beam Irradiation: A Synergetic Computational and Experimental Study. *Inorg. Chem.* **2016**, *55*, 8661.
(23) Alvarez Roca, R.; Lemos, P. S.; Andrés, J.; Longo, E. Formation of Ag Nanoparticles on Metastable $\beta$-Ag2WO4Microcrystals Induced by Electron Irradiation. *Chem. Phys. Lett.* **2016**, *644*, 68.
(24) Fabbro, M. T.; Saliby, C.; Rios, L. R.; La Porta, F. A.; Gracia, L.; Li, M. S.; Andrés, J.; Santos, L. P. S.; Longo, E. Identifying and Rationalizing the Morphological, Structural, and Optical Properties of $\beta$-Ag2MoO4 Microcrystals, and the Formation Process of Ag Nanoparticles on Their Surfaces: Combining Experimental Data and First-Principles Calculations. *Sci. Technol. Adv. Mater.* **2015**, *16*, 065002.
(25) Andrés, J.; Ferrer, M. M.; Gracia, L.; Beltran, A.; Longo, V. M.; Cruvinel, G. H.; Tranquilin, R. L.; Longo, E. A Combined Experimental and Theoretical Study on the Formation of Ag Filaments on $\beta$-Ag2MoO4 Induced by Electron Irradiation. *Part. Part. Syst. Charact.* **2015**, *32*, 646.
(26) Botelho, G.; Sczancoski, J. C.; Andres, J.; Gracia, L.; Longo, E. Experimental and Theoretical Study on the Structure, Optical Properties, and Growth of Metallic Silver Nanostructures in Ag3PO4. *J. Phys. Chem. C* **2015**, *119*, 6293.
(27) De Oliveira, R. C.; Assis, M.; Teixeira, M. M.; Da Silva, M. D. P.; Li, M. S.; Andres, J.; Gracia, L.; Longo, E. An Experimental and Computational Study of $\beta$-AgVO3: Optical Properties and Formation of Ag Nanoparticles. *J. Phys. Chem. C* **2016**, *120*, 12254.
(28) Fabbro, M. T.; Gracia, L.; Silva, G. S.; Santos, L. P. S.; Andrés, J.; Cordoncillo, E.; Longo, E. Understanding the Formation and Growth of Ag Nanoparticles on Silver Chromate Induced by Electron Irradiation in Electron Microscope: A Combined Experimental and Theoretical Study. *J. Solid State Chem.* **2016**, *239*, 220.
(29) Assis, M.; et al. Ag Nanoparticles/AgX (X = Cl, Br and I) Composites with Enhanced Photocatalytic Activity and Low Toxicological Effects. *ChemistrySelect* **2020**, *5*, 4655.
(30) Osman, H. H.; Andrés, J.; Salvadó, M. A.; Recio, J. M. Chemical Bond Formation and Rupture Processes: An Application of DFT-Chemical Pressure Approach. *J. Phys. Chem. C* **2018**, *122*, 21216.
(31) Cabral, L.; et al. Evidence for the Formation of Metallic in after Laser Irradiation of InP. *J. Appl. Phys.* **2019**, *126*, 025902.
(32) Assis, M.; Carvalho De Oliveira, M.; Machado, T. R.; Macedo, N. G.; Costa, J. P. C.; Gracia, L.; Andrés, J.; Longo, E. In Situ Growth of Bi Nanoparticles on NaBiO 3, $\delta$-, and $\beta$-Bi 2 O 3 Surfaces: Electron Irradiation and Theoretical Insights. *J. Phys. Chem. C* **2019**, *123*, 5023.
(33) Assis, M.; Cordoncillo, E.; Torres-Mendieta, R.; Beltrán-Mir, H.; Mínguez-Vega, G.; Gouveia, A. F.; Leite, E.; Andrés, J.; Longo, E. Laser-Induced Formation of Bismuth Nanoparticles. *Phys. Chem. Chem. Phys.* **2018**, *20*, 13693.
(34) Da Silva, E. Z.; Faccin, G. M.; Machado, T. R.; Macedo, N. G.; De Assis, M.; Maya-Johnson, S.; Sczancoski, J. C.; Andrés, J.; Longo, E.; San-Miguel, M. A. Connecting Theory with Experiment to Understand the Sintering Processes of Ag Nanoparticles. *J. Phys. Chem. C* **2019**, *123*, 11310.
(35) de Campos da Costa, J. P.; Teodoro, V.; Assis, M.; Bettini, J.; Andrés, J.; Pereira do Carmo, J. P.; Longo, E. A Scalable Electron Beam Irradiation Platform Applied for Allotropic Carbon Transformation. *Carbon N. Y.* **2021**, *174*, 567.
(36) Toulemonde, M.; Dufour, C.; Paumier, E. Transient Thermal Process after a High-Energy Heavy-Ion Irradiation of Amorphous Metals and Semiconductors. *Phys. Rev. B* **1992**, *46*, 14362.
(37) Mermin, N. D. Thermal Properties of the Inhomogeneous Electron Gas. *Phys. Rev.* **1965**, *137*, A1441.
(38) Kresse, G.; Hafner, J. Ab Initio Molecular Dynamics for Liquid Metals. *Phys. Rev. B* **1993**, *47*, 558.
(39) Alavi, A.; Kohanoff, J.; Parrinello, M.; Frenkel, D. Ab Initio Molecular Dynamics with Excited Electrons. *Phys. Rev. Lett.* **1994**, *73*, 2599.
(40) Zhao, S.; Zhang, Y.; Weber, W. J. Ab Initio Study of Electronic Excitation Effects on SrTiO3. *J. Phys. Chem. C* **2017**, *121*, 26622.
(41) Cabral, L.; Andrés, J.; Longo, E.; San-Miguel, M. A.; da Silva, E. Z. Formation of Metallic Ag on AgBr by Femtosecond Laser Irradiation. *Physchem* **2022**, *2*, 179.
(42) Silvestrelli, P. L.; Alavi, A.; Parrinello, M.; Frenkel, D. Ab Initio Molecular Dynamics Simulation of Laser Melting of Silicon. *Phys. Rev. Lett.* **1996**, *77*, 3149.
(43) Flores, E. M.; Moreira, M. L.; Piotrowski, M. J. Structural and Electronic Properties of Bulk ZnX (X = O, S, Se, Te), ZnF2, and ZnO/ZnF2: A DFT Investigation within PBE, PBE + U, and Hybrid HSE Functionals. *J. Phys. Chem. A* **2020**, *124*, 3778.
(44) Jain, M.; Chelikowsky, J. R.; Louie, S. G. Reliability of Hybrid Functionals in Predicting Band Gaps. *Phys. Rev. Lett.* **2011**, *107*, 216806.
(45) Andrés, J.; et al. Structural and Electronic Analysis of the Atomic Scale Nucleation of Ag on $\alpha$-Ag2WO4 Induced by Electron Irradiation. *Sci. Rep.* **2014**, *4*, 5391.
(46) Pereira, W. da S.; Andrés, J.; Gracia, L.; San-Miguel, M. A.; da Silva, E. Z.; Longo, E.; Longo, V. M. Elucidating the Real-Time Ag Nanoparticle Growth on $\alpha$-Ag 2 WO 4 during Electron Beam Irradiation: Experimental Evidence and Theoretical Insights. *Phys. Chem. Chem. Phys.* **2015**, *17*, 5352.
(47) Billinge, S. J. L.; Kanatzidis, M. G. Beyond Crystallography: The Study of Disorder, Nanocrystallinity and Crystallographically Challenged Materials with Pair Distribution Functions. *Chem. Commun.* **2004**, *4*, 749.
(48) Souza Junior, J. B.; Schleder, G. R.; Bettini, J.; Nogueira, I. C.; Fazzio, A.; Leite, E. R. Pair Distribution Function Obtained from Electron Diffraction: An Advanced Real-Space Structural Characterization Tool. *Matter* **2021**, *4*, 441.
(49) Chen, M.; Dyer, J. E.; Li, K.; Dixon, D. A. Prediction of Structures and Atomization Energies of Small Silver Clusters, (Ag)n, $n < 100$. *J. Phys. Chem. A* **2013**, *117*, 8298.
(50) Hagen, S.; Schubert, H.; Maichle-Mössmer, C.; Pantenburg, I.; Weigend, F.; Wesemann, L. Silver Aggregation Caused by Stanna-Closo-Dodecaborate Coordination: Syntheses, Solid-State Structures and Theoretical Studies. *Inorg. Chem.* **2007**, *46*, 6775.
(51) Longo, E.; Cavalcante, L. S.; Volanti, D. P.; Gouveia, A. F.; Longo, V. M.; Varela, J. A.; Orlandi, M. O.; Andrés, J. Direct in Situ Observation of the Electron-Driven Synthesis of Ag Filaments on $\alpha$-Ag2 WO4 Crystals. *Sci. Rep.* **2013**, *3*, 1676.
(52) Longo, E.; Avansi, W.; Bettini, J.; Andrés, J.; Gracia, L. In Situ Transmission Electron Microscopy Observation of Ag Nanocrystal Evolution by Surfactant Free Electron-Driven Synthesis. *Sci. Rep.* **2016**, *6*, 21498.
(53) Paulo de Campos da Costa, J.; Assis, M.; Teodoro, V.; Rodrigues, A.; Cristina de Foggi, C.; San-Miguel, M. A.; Pereira do Carmo, J. P.; Andrés, J.; Longo, E. Electron Beam Irradiation for the Formation of Thick Ag Film on Ag3PO4. *RSC Adv.* **2020**, *10*, 21745.
(54) Wu, M.; Wu, Y. F.; Ma, Y. Anomalous Bond-Length Behaviors of Solid Halogens under Pressure. *Chinese Phys. B* **2021**, *30*, 076401.
(55) Wu, M.; Tse, J. S.; Pan, Y. Anomalous Bond Length Behavior and a New Solid Phase of Bromine under Pressure. *Sci. Rep.* **2016**, *6*, 25649.
(56) Shi, J.; et al. Halogen Molecular Modifications at High Pressure: The Case of Iodine. *Phys. Chem. Chem. Phys.* **2021**, *23*, 3321.
(57) Schleder, G. R.; Padilha, A. C. M.; Acosta, C. M.; Costa, M.; Fazzio, A. From DFT to Machine Learning: Recent Approaches to Materials Science - A Review. *JPhys. Mater.* **2019**, *2*, 032001.
(58) Guo, K.; Yang, Z.; Yu, C. H.; Buehler, M. J. Artificial Intelligence and Machine Learning in Design of Mechanical Materials. *Mater. Horizons* **2021**, *8*, 1153.


https://doi.org/10.1021/acs.nanolett.3c04130
*Nano Lett.* XXXX, XXX, XXX−XXX